Inorg. Chem. **2002**, *41*, 1523–1533

Homologous Series of Redox-Active, Dinuclear Cations $[M_2(O_2CCH_3)_2(pynp)_2]^{2+}$ (M = Mo, Ru, Rh) with the Bridging Ligand 2-(2-Pyridyl)-1,8-naphthyridine (pynp)

Cristian Saul Campos-Fernández, Lisa M. Thomson,† José Ramón Galán-Mascarós, Xiang Ouyang, and Kim R. Dunbar*

Department of Chemistry and Laboratory for Molecular Simulation, Texas A&M University, College Station, Texas 77842-3012

Received September 25, 2001

A homologous series of dinuclear compounds with the bridging ligand 2-(2-pyridyl)-1,8-naphthyridine (pynp) has been prepared and characterized by X-ray crystallographic and spectroscopic methods. $[Mo_2(O_2CCH_3)_2(pynp)_2][BF_4]_2 \cdot 3CH_3CN$ (**1**) crystallizes in the monoclinic space group $P2_1/c$ with $a = 15.134(5)$ Å, $b = 14.301(6)$ Å, $c = 19.990(6)$ Å, $\beta = 108.06(2)°$, $V = 4113(3)$ Å^3, and $Z = 4$. $[Ru_2(O_2CCH_3)_2(pynp)_2][PF_6]_2 \cdot 2CH_3OH$ (**2**) crystallizes in the monoclinic space group $C2/c$ with $a = 14.2228(7)$ Å, $b = 20.3204(9)$ Å, $c = 14.1022(7)$ Å, $\beta = 95.144(1)°$, $V = 4059.3(3)$ Å^3, and $Z = 4$. $[Rh_2(O_2CCH_3)_2(pynp)_2][BF_4]_2 \cdot C_7H_8$ (**3**) crystallizes in the monoclinic space group $C2/c$ with $a = 13.409(2)$ Å, $b = 21.670(3)$ Å, $c = 13.726(2)$ Å, $\beta = 94.865(2)°$, $V = 3973.9(8)$ Å^3, and $Z = 4$. A minor product, $[Rh_2(O_2CCH_3)_2(pynp)_2(CH_3CN)_2][BF_4][PF_6] \cdot 2CH_3CN$ (**4**), was isolated from the mother liquor after crystals of **3** had been harvested; this compound crystallizes in the triclinic space group, $P\bar{1}$ with $a = 12.535(3)$ Å, $b = 13.116(3)$ Å, $c = 13.785(3)$ Å, $\alpha = 82.52(3)°$, $\beta = 77.70(3)°$, $\gamma = 85.76(3)°$, $V = 2193.0(8)$ Å^3, and $Z = 2$. Compounds **1**–**3** constitute a convenient series for probing the influence of the electronic configuration on the extent of mixing of the M–M orbitals with the π system of the pynp ligand. Single point energy calculations performed on **1**–**3** at the B3LYP level of theory lend insight into the bonding in these compounds and allow for correlations to be made with electronic spectral data. Although purely qualitative in nature, the values for normalized change in orbital energies (NCOE) of the frontier orbitals before and after reduction are in agreement with the observed differences in reduction potentials as determined by cyclic voltammetry.

Introduction

The study of light-harvesting properties of metal assemblies that contain nitrogen π ligands,[1–4] particularly those based on the $[Ru(bpy)_3]^{2+}$ prototype, is an extremely active area of current research.[2] In the pursuit of extended arrays with electronic communication between the individual units, few researchers have focused on building blocks that contain metal−metal bonds. Given the extensive redox chemistry exhibited by many dinuclear complexes, and the demonstrated possibility for coupling these units electronically, their incorporation into extended arrays is an area with much potential.[3]

Mononuclear complexes with nitrogen heterocyclic ligands exhibit rich electrochemistry and interesting optical proper-

* To whom correspondence should be addressed. Phone: (979) 845-5235. Fax: (979) 845-7177. E-mail: dunbar@mail.chem.tamu.edu.
† E-mail: mouse@mail.chem.tamu.edu.

(1) Sutin, N.; Creutz, C. *Pure Appl. Chem.* **1980**, *52*, 2717.
(2) (a) Kaes, C.; Katz, A.; Hosseini, W. *Chem. Rev.* **2000**, *100*, 3553. (b) Decloitre, Y.; Thummel, R. *Inorg. Chim. Acta* **1987**, *128*, 245. (c) Ortmans, I.; Moucheron, C.; Mesmaeker, A. K-.D. *Coord. Chem. Rev.* **1998**, *168*, 233. (d) Baggio, R.; Garland, M. T.; Perec, M. *Inorg. Chim. Acta* **2000**, *310*, 103.
(3) (a) Cotton, F. A.; Lin, C.; Murillo, C. A. *J. Chem. Soc., Dalton Trans.* **1998**, 3151. (b) Weseman, J. L.; Chisholm, M. H. *Inorg. Chem.* **1997**, *36*, 3258. (c) Cayton, R. R. H.; Chisholm, M. H.; Huffman, J. C.; Lobkovsky, E. B. *J. Am. Chem. Soc.* **1991**, *113*, 8709. (d) Chisholm, M. H.; Glasgow, K. C.; Klein, J.; Macintosh, A. M.; Peters, D. G. *Inorg. Chem.* **2000**, *39*, 4354. (e) Cotton, F. A.; Dikarev, E. V.; Petrukhina, M. A.; Taylor, R. E. *J. Am. Chem. Soc.* **2001**, *123*, 5831. (f) Cotton, F. A.; Donahue, J. P.; Murillo, C. A. *Inorg. Chem.* **2001**, *40*, 2229. (g) Cotton, F. A.; Lin, C.; Murillo, C. A. *J. Am. Chem. Soc.* **2001**, *123*, 2670. (h) Cotton, F. A.; Donahue, J. P.; Lin, C.; Murillo, C. A. *Inorg. Chem.* **2001**, *40*, 1234. (i) Bera, J. K.; Angaridis, P.; Cotton, F. A.; Petrukhina, M. A.; Fanwick, P. E.; Walton, R. A. *J. Am. Chem. Soc.* **2001**, *123*, 1515. (j) Wesemann, J. L.; Chisholm, M. H. *Inorg. Chem.* **1997**, *36*, 3258.
(4) (a) Caluwe, P.; Evens, G. *Macromolecules* **1979**, *12*, 803. (b) Tikkanen, W.; Binamira-Soriaga, E.; Kaska, W.; Ford, P. *Inorg. Chem.* **1984**, *23*, 141. (c) Tikkanen, W.; Binamira-Soriaga, E.; Kaska, W.; Ford, P. *Inorg. Chem.* **1983**, *22*, 1147. (d) Thummel, R. P.; Lefoulon, F.; Williamson, D.; Chavan, M. *Inorg. Chem.* **1986**, *25*, 1675. (e) Binamira-Soriaga, E.; Keder, N. L.; Kaska, W. C.; McLoughlin, M. A.; Keder, N. L.; Harrison, W. T. A.; Stucky, G. D. *Inorg. Chem.* **1990**, *29*, 2238. (f) Binamira-Soriaga, E.; Keder, N. L.; Kaska, W. C. *Inorg. Chem.* **1990**, *29*, 3167. (g) Binamira-Soriaga, E.; Sprouse, S. D.; Watts, R. J.; Kaska, W. C. *Inorg. Chim. Acta.* **1984**, *84*, 135. (h) Thummel, R. P.; Decloitre, Y. *Inorg. Chim. Acta* **1987**, *128*, 245. (i) Collin, J.-P.; Jouaiti, A.; Sauvage, J.-P.; Kaska, W. C.; McLoughlin, M. A.; Keder, N. L.; Harrison, W. T. A.; Stucky, G. D. *Inorg. Chem.* **1990**, *29*, 2238.

10.1021/ic010996u CCC: $22.00
Published on Web 03/18/2002

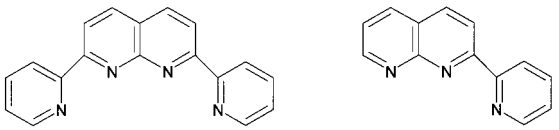

bpnp pynp

Figure 1. Schematic drawings of the pynp and bpnp molecules.

ties; therefore, it seemed to us that a logical extrapolation of this chemistry to metal−metal bonded compounds is to use bridging ligands such as 2-(2-pyridyl)-1,8-naphthyridine (pynp)[4] and 2,7-bis(2-pyridyl)-1,8-naphthyridine (bpnp)[4a,d−g] (Figure 1). The crescent-shaped pynp and bpnp molecules are relatively rigid ligands based on the naphthyridine unit, with one and two pyridine substituents, respectively. The pynp ligand (Figure 1) has been observed to behave as a tridentate combination bridging/chelating ligand in $[Rh_2(O_2CCH_3)_2(pynp)_2]^{2+}$ [4b] and as a chelating, bpy ligand in $[Rh_2(pynp)_3Cl_2][PF_6]\cdot CH_3CN$.[5] Although these compounds were found to exhibit interesting electronic properties, no additional reports of M−M bonded pynp compounds have appeared in the literature. Moreover, only one X-ray structure has been reported to our knowledge.[4c] In the present study, we report the isolation of the homologous series $[M_2(O_2CCH_3)_2(pynp)_2][BF_4]_2$ (M = Mo, Ru, and Rh) from reactions of 2-(2-pyridyl)-1,8-naphthyridine (pynp) with $[Mo_2(O_2CCH_3)_2(CH_3CN)_6][BF_4]_2$, $[Rh_2(O_2CCH_3)_2(CH_3CN)_6][BF_4]_2$, and $Ru_2(O_2CCH_3)_4Cl$.[6] A comparison of the structural and bonding variations within this series was made on the basis of X-ray crystallographic studies, electrochemical properties, and density functional calculations.

Experimental Section

All manipulations were performed under an inert atmosphere with the use of standard Schlenk line techniques. Acetonitrile was freshly distilled over 3 Å molecular sieves, and methanol was distilled over NaOMe. The solvents diethyl ether and toluene were freshly distilled over Na/K amalgam. The ligand 2-(2-pyridyl)-1,8-naphthyridine (pynp) was prepared by a modified literature procedure.[7] The starting materials $[Rh_2(O_2CCH_3)_2(CH_3CN)_6][BF_4]_2$,[8] $[Mo_2(O_2CCH_3)_2(CH_3CN)_6][BF_4]_2$,[8,9] and $[Ru_2(O_2CCH_3)_4Cl]$[10] were prepared by literature methods.

Physical Measurements. ^{1}H NMR spectra were obtained on a Varian VXR 300-MHz spectrometer Gemini-200. Electrochemical measurements were carried out by using an H−CH Electrochemical Analyzer model 620A. Cyclic voltammetric measurements were performed in CH_3CN with 0.1 M tetra-*n*-butylammonium hexafluorophosphate ($TBAPF_6$) as the supporting electrolyte. The working electrode was a BAS Pt disk electrode, the reference electrode was Ag/AgCl, and the auxiliary electrode was a Pt wire. The ferrocene couple occurs at $E_{1/2} = +0.52$ V versus Ag/AgCl under the same experimental conditions. Magnetic susceptibility measurements were obtained with the use of a Quantum Design SQUID magnetometer MPMS-XL housed in the Department of Chemistry at Texas A&M University. Data were collected in the temperature range 1.8−350 K at 1000 G on finely divided polycrystalline samples. The raw data were corrected for the contribution of the sample holder and for the diamagnetism of the constituent atoms by the use of Pascal constants.[11]

Theoretical Studies. The molecules $[M(O_2CCH_3)_2(pynp)_2]^{2+}$ ($M = Mo^{II}$, Ru^{II}, Rh^{II}) were characterized at the X-ray crystal structure geometries (without solvent molecules) using density functional theory (DFT)[12] with the Becke3 hybrid exchange functional and the Lee−Yang−Parr correlation functional (B3LYP).[13] All calculations were performed with the Gaussian 98 (G98)[14] suite of programs using the all electron split-valence double-ζ basis set of Dunning[15] for all atoms except the metals. The double-ζ basis set of Hay and Wadt with a small core (1s2s2p3s3p3d) effective core potential (ECP)[16] was used for Mo, Ru, and Rh. The basis set used to describe the compounds is relatively small; nevertheless the calculations involved 452 basis functions. Calculations on species with unpaired electrons (open shell) were performed using unrestricted B3LYP (UB3LYP); the α and β molecular orbitals were optimized independently.

To analyze the observed electrochemical potentials in the cyclic voltammograms for this series of compounds, single point energy calculations were performed for five oxidation states of the diruthenium compound $[Ru_2]^{(2+/1+/0/1-/2-)}$ and three oxidation states of the dimolybdenum and dirhodium compounds ($[Mo_2]^{(2+/0/2-)}$, $[Rh_2]^{(2+/0/2-)}$). The reason that only three oxidation states were calculated for Mo and Rh will be discussed in the section that pertains to the correlation of the calculations with the electrochemistry of the compounds. In simplified terms, the electrochemical potential observed for two $1e^-$ reductions depends on three main factors; these are (1) the absolute energy of the molecular orbital to be occupied by the added electrons, (2) the relaxation of the molecular orbitals upon the addition of the first electron, and (3) the change in solvation upon the addition of the electrons. To estimate the relaxation of the orbital energy using the B3LYP calculations, the energy of the molecular orbital to be occupied with the addition of the first electron was compared to an occupied orbital before and after reduction. Simply put, we calculated the difference of the ΔE(LUMO − HOMO) of the unreduced species

(5) Baker, A. T.; Tikkanen, W. R.; Kaska, W. C.; Ford, P. C. *Inorg. Chem.* **1984**, *23*, 3254.
(6) A preliminary communication on these series of compounds has appeared: Campos-Fernández, C. S.; Ouyang, X.; Dunbar, K. R. *Inorg. Chem.* **2000**, *39*, 2432.
(7) Majewicz, T. C.; Caluwe, P. *J. Org. Chem.* **1974**, *39*, 720.
(8) Pimblett, G.; Garner, C. D.; Clegg, W. *J. Chem. Soc., Dalton Trans.* **1986**, 1257.
(9) Cotton, F. A.; Reid, A. H.; Schwotzer, W. *Inorg. Chem.* **1985**, *24*, 3965.
(10) Martin, D. S.; Newman, R. A.; Vlasnik, I. M. *Inorg. Chem.* **1980**, *19*, 3404.
(11) *Theory and Applications of Molecular Paramagnetism*; Boudreaux, E. A., Mulay, L. N., Eds.; John Wiley & Sons: New York, 1976.
(12) Parr, R. G.; Yang, W. *Density-functional theory of atoms and molecules*; Oxford University Press: Oxford, 1989.
(13) (a) Becke, A. D. *J. Chem. Phys.* **1993**, *98*, 5648. (b) Lee, C.; Yang, W.; Parr, R. G. *Phys. Rev. B* **1998**, *37*, 785.
(14) Frisch, M. J.; Trucks, G. W.; Schlegel, H. B.; Scuseria, G. E.; Robb, M. A.; Cheeseman, J. R.; Zakrzewski, V. G.; Montgomery, J. A.; Stratmann, R. E.; Burant, J. C.; Dapprich, S.; Millam, J. M.; Daniels, A. D.; Kudin, K. N.; Strain, M. C.; Farkas, O.; Tomasi, J.; Barone, V.; Cossi, M.; Cammi, R.; Mennucci, B.; Pomelli, C.; Adamo, C.; Clifford, S.; Ochterski, J.; Petersson, G. A.; Ayala, P. Y.; Cui, Q.; Morokuma, K.; Malick, D. K.; Rabuck, A. D.; Raghavachari, K.; Foresman, J. B.; Cioslowski, J.; Ortiz, J. V.; Stefanov, B. B.; Liu, G.; Liashenko, A.; Piskorz, P.; Komaromi, I.; Gomperts, R.; Martin, R. L.; Fox, D. J.; Keith, T.; Al-Laham, M. A.; Peng, C. Y.; Nanayakkara, A.; Gonzalez, C.; Challacombe, M.; Gill, P. M. W.; Johnson, B. G.; Chen, W.; Wong, M. W.; Andres, J. L.; Head-Gordon, M.; Replogle, E. S.; Pople, J. A. *Gaussian 98*, revision A.6; Gaussian, Inc.: Pittsburgh, PA, 1998.
(15) Dunning, T. H., Jr.; Hay, P. J. *Modern Theoretical Chemistry*; Schaefer, H. F., III, Ed.; Plenum: New York, 1976, pp 1−28.
(16) (a) Hay, P. J.; Wadt, W. R. *J. Chem. Phys.* **1985**, *82*, 270. (b) Wadt, W. R.; Hay, P. J. *J. Chem. Phys.* **1985**, *82*, 284. (c) Hay, P. J.; Wadt, W. R. *J. Chem. Phys.* **1985**, *82*, 299.

and the ΔE(HOMO − (HOMO−1)) of the reduced species. These values should be proportional to the amount of relaxation in the orbital energies upon reduction, but they do not correlate well with the electrochemical potentials because of the lack of solvation of the charge in the gas-phase calculations. In general, solvation should dampen the change in orbital energies upon reduction; therefore, to incorporate solvation effects, the value for the relaxation energy was divided by the average of ΔE(LUMO − HOMO) of the unreduced species and the ΔE(HOMO − (HOMO-1)) of the reduced species. The final equation used to correlate the single point energy calculations with the electrochemistry is given in eq 1, and the value is designated as the normalized change in orbital energies (NCOE). Because the NCOE value should be proportional to the orbital energy, relaxation, and solvation effects, it should also be proportional to the observed electrochemical potentials, that is, the larger the NCOE, the larger the difference in the electrochemical potential between two oxidation states.

$$\mathrm{NCOE} = \frac{(E^{2+}_{\mathrm{HOMO}} - E^{2+}_{\mathrm{LUMO}})(E^{0}_{\mathrm{HOMO-1}} - E^{0}_{\mathrm{HOMO}})}{1/2((E^{2+}_{\mathrm{HOMO}} - E^{2+}_{\mathrm{LUMO}})(E^{0}_{\mathrm{HOMO-1}} - E^{0}_{\mathrm{HOMO}}))} \quad (1)$$

Syntheses. 2-(2-Pyridyl)-1,8-naphthridine (pynp). The preparation of the pynp ligand requires the use of the precursor 2-aminonicotinaldehyde, a reagent that must be freshly prepared and used immediately after isolation to avoid self-condensation side reactions.

2-Aminonicotinaldehyde. The method of Caluwe and coworkers[7] was followed with some modifications. Nicotinamide (9.1 g, 0.07 mmol) was intimately mixed with 13.0 g (0.11 mmol) of ammonium sulfamate in a 500 mL round-bottomed flask equipped with a condenser. The temperature was slowly increased to 150 °C until the entire solid had melted. The reaction temperature was further increased to 200 °C, after which time the molten mixture was refluxed for 8.5 h. The grayish-white solid obtained from this procedure was washed with copious amounts of water and diethyl ether to remove unreacted nicotinamide and sulfamate. The remaining solid was refluxed in 75 mL of 4 N HCl for 6.5 h, and the solution was made basic (pH ∼9.0) by adding a saturated NaOH solution dropwise. The resulting solution was subjected to four extractions with diethyl ether, and the combined extracts were dried over anhydrous $MgSO_4$ for 1 h. The diethyl ether was evaporated, and the remaining light yellow solid was sublimed at 60 °C under vacuum to obtain pure 2-aminonicotinaldehyde. Yield 3.1 g (34%). This product was stored under an inert atmosphere at 0 °C to avoid self-condensation reactions. IR data (KBr pellet cm^{-1}): 3412 (br, w), 2924 (br,w), 2750 (w), 1669 (w), 1624 (w), 1568 (w), 1458 (w), 1402 (w), 1377 (w), 1296 (w), 1273 (w), 1194 (w), 1136 (w), 912 (w), 775 (w), 675 (w), 623 (w). ^{1}H NMR spectrum in $CDCl_3$ at 25 °C: δ 9.82 (s, OH), 8.22 (dd), 7.78 (dd), 6.95 (b), 6.72 (dd) ppm.

2-(2-Pyridyl)-1,8-naphthyridine (pynp). An amount of freshly prepared 2-aminonicotinaldehyde (1.6 g, 14.8 mmol) was placed in a 100 mL round-bottomed Schlenk flask under nitrogen and dissolved in 25 mL of freshly distilled ethanol. To this solution was added 1.0 mL of 2-acetyl-pyridine. The solution was refluxed under nitrogen and treated with one drop of a freshly prepared methanol solution saturated with NaOH. A color change from yellow to pale brown-yellow immediately ensued, and the solution was refluxed overnight under nitrogen. The solution was concentrated to one-half of its original volume which led to the formation of white crystals after a few hours. Yield 1.1 g (43%). (KBr pellet cm^{-1}): 1550(m), 1520 (w), 1470 (s), 1350 (m), 1050 (w), 850 (w), 800 (m), 750 (w). ^{1}H NMR spectrum in CD_3CN at 25 °C: δ 9.1 (q), 8.75 (m), 8.68 (d,d), 8.45 (d), 8.36 (d,d), 7.95 (t,d), 7.56 (q), 7.48 (m) ppm.

$[Mo_2(O_2CCH_3)_2(pynp)_2][BF_4]_2$ (1). A sample of $[Mo_2(O_2CCH_3)_2(CH_3CN)_6][BF_4]_2$ (0.2 g, 0.27 mmol) dissolved in 20 mL of CH_3CN was treated with 114 mg (55 mmol) of pynp, which led to a color change from light pink to dark green. After 12 h, the solution was concentrated, and diethyl ether was added to the point of saturation. The solution was then placed in a refrigerator for 12 h to yield green platelets. Yield 0.145 g (75%). IR (Nujol, KBr): 2924 (br, s), 2725 (w), 1606 (w), 1557 (w), 1518 (w), 1458 (s), 1377 (s), 1316 (w), 1263 (w), 1217 (w), 1146 (w), 1057 (br,s), 854(w), 816 (w), 781 (w), 721 (w), 679 (w), 521 (w) cm^{-1}. ^{1}H NMR spectrum in CD_3CN at 25 °C: δ 9.05 (d, pynp), 8.85 (dd, pynp), 8.68 (d), 8.2 (td, pynp), 7.72 (m, pynp), 7.66 (m, pynp), 7.52 (m, pynp), 2.65 (s,CH_3-acetate) ppm. Anal. Found: C, 39.94; H, 2.65; N, 9.18%. Calcd for $C_{30}H_{24}B_2F_8Mo_2N_6O_4$: C, 40.12; H, 2.69; N, 9.36%.

$[Ru_2(O_2CCH_3)_2(pynp)_2][PF_6]_2$ (2). The starting material $[Ru_2(O_2CCH_3)_4Cl]$ (0.150 g, 0.32 mmol) and $TBAPF_6$ (0.250 g, 0.64 g) were dissolved in 20 mL of MeOH and treated with 0.131 g (0.64 mmol) of pynp. The initial dark brown solution instantaneously turned to a dark blue color. This solution was stirred overnight, and the volume was decreased to ∼10 mL, after which time diethyl ether was added to produce a dark blue crystalline powder. Yield 0.103 g (60%). IR (Nujol, KBr): 2700 (br,s), 2350 (w), 1450 (s), 1380 (s), 1300 (br,w), 845 (br,s), 780 (br,s), 710 (w), 580 (w). The ^{1}H NMR signals of the product were broad and featureless. Anal. Found: C, 34.77; H, 2.38; N, 7.94%. Calcd for $C_{30}H_{24}P_2F_{12}Ru_2N_6O_4$: C, 35.17; H, 2.36; N, 8.20%.

$[Rh_2(O_2CCH_3)_2(pynp)_2][BF_4]_2$ (3). A sample of $[Rh_2(O_2CCH_3)_2(CH_3CN)_6][BF_4]_2$ (0.1 g, 0.13 mmol) was treated with 0.056 g (0.27 mmol) of pynp in 20 mL of CH_3CN which led to an instantaneous color change from pale red to intense red. After stirring overnight, the volume was reduced to 5 mL, and the solution was layered with toluene. A crop of red crystals was harvested after 3 days. Yield 0.077 g (70%). IR (Nujol, KBr): 2926 (br, s), 2725 (w), 1604 (w), 1650 (w), 1523 (w), 1462 (s), 1377 (w), 1315 (w), 1265 (w), 1147 (w), 1059 (w), 1012 (w), 841 (w), 779 (w), 736(w), 715 (w), 559 (w). ^{1}H NMR spectrum in CD_3CN at 25 °C: δ 9.70 (d, pynp), 8.87 (dd, pynp), 8.70 (d, pynp), 8.60 (m, pynp), 8.45 (dd, pynp), 8.35 (td, pynp), 7.48 (q, pynp), 2.25 (s,CH_3-acetate) ppm. Anal. Found: C, 38.99; H, 3.07; N, 9.65%. Calcd for $C_{30}H_{24}B_2F_8Rh_2N_6O_4$: C, 39.51%; H, 2.65; N, 9.22%.

X-ray Data Collection and Refinement. Geometric and intensity data for compound **1** were collected on a Rigaku AFC6S diffractometer equipped with a graphite-monochromated Mo Kα (λ_α = 0.71069 Å) radiation source. All calculations were performed with VAX computers on a cluster network using Texsan software package of the Molecular Structure Corporation.[17] X-ray structural studies for compounds **2**−**4** were performed on a SMART 1K area detector diffractometer equipped with graphite monochromated Mo Kα radiation (λ_α = 0.71073 Å). The frames were integrated in the Siemens SAINT software package,[18] and the data were solved using the direct-methods program SHELXS-97.[19] Crystal data and main refinement parameters are listed for compounds **1**−**4** in Table 1.

$[Mo_2(O_2CCH_3)_2(pynp)_2][BF_4]_2 \cdot 3CH_3CN$ (1). X-ray quality crystals were obtained within 3 days from a saturated solution of

(17) *TEXSAN-TEXRAY Structure Analysis Package*; Molecular Structure Corporation: The Woodlands, TX, 1985.
(18) *SAINT, Program for area detector absorption correction*; Siemens Analytical X-ray Instruments Inc.: Madison, WI , 1994−1996.
(19) Sheldrick, G. M. *SHELXL−97, Program for Crystal Structure Determination*; University of Göttingen: Göttingen, Germany, 1997.

Table 1. Crystallographic Data for Compounds **1**−**4**

	1	**2**	**3**	**4**
empirical formula	$C_{36}H_{33}B_2F_8N_9O_4Mo_2$	$C_{32}H_{32}P_2F_{12}N_6O_6Ru_2$	$C_{37}H_{32}B_2F_8N_6O_4Rh_2$	$C_{38}H_{36}P_1B_1F_{10}N_{10}O_4Rh_2$
fw	1021.21	1004.87	1004.11	1133.61
space group	*P*21/*c*	*C*2/*c*	*C*2/*c*	$P\bar{1}$
a, Å	15.134(5)	14.2228(7)	13.409(2)	12.535(3)
b, Å	14.301(6)	20.3204(9)	21.670(3)	13.116(3)
c, Å	19.990(6)	14.1022(7)	13.726(2)	13.785(3)
α	90	90	90	82.52(3)
β	108.06(1)	95.144(1)	94.865(2)	77.70(3)
γ	90	90	90	85.76(3)
V, Å^3	4113(3)	4059.3(3)	3973.9(8)	2.193.0(8)
Z	4	8	4	2
D g/cm^3	1.649	1.808	1.685	1.713
μ (mm^{-1})	0.697	0.931	0.916	0.884
total data	7493	9867	7670	23918
unique data	7200	3429	3203	9970
R indices	R1 = 0.0598	R1 = 0.617	R1 = 0.1062	R1 = 0.0678
$[I > 2\sigma(I)]^{a,b}$	wR2 = 0.1690	wR2 = 0.170	wR2 =0.2365	wR2 = 0.1642
R indices	R1 = 0.1545	R1 = 0.0812	R1 = 0.1773	R1 = 0.1250
(all data)	wR2 = 0.2064	wR2 = 0.1798	wR2 = 0.2809	wR2 = 0.1881
GOF	1.017	1.078	1.117	0.980

[a] $R1 = \sum||F_o| - |F_c||/\sum|F_o|$. [b] $wR2 = [\sum[w(F_o^2 - F_c^2)^2]/\sum[w(F_o^2)^2]]^{0.5}$.

the title compound in acetonitrile with diethyl ether at −5 °C. A green rectangular crystal of dimensions 0.80 × 0.4 × 0.25 mm^3 was covered with silicone grease and mounted on the tip of a glass fiber. Cell constants were obtained from a least squares refinement using 25 carefully centered reflections in the range 29° ≤ 2θ ≤ 37°. Data were collected at 173 ± 2 K by using the ω-scan method, in the range 4° ≤ 2θ ≤ 47°. A total of 7493 reflections were collected, of which 7200 were unique. The final full-matrix, least-squares refinement was based on 4162 observed reflections that were used to fit 550 parameters to give R1 = 0.0598 and wR2 = 0.1690. The goodness-of-fit index was 0.999, and the highest peak in the final difference map was 1.017 e$^-$/Å^{-3}.

$[Ru_2(O_2CCH_3)_2(pynp)_2][PF_6]_2\cdot 2CH_3OH$ (2). X-ray quality crystals were grown by layering a methanol solution of the title compound with toluene. A blue platelet of dimensions 0.11 × 0.07 × 0.05 mm^3 was secured on the tip of a glass fiber with silicone grease and placed in a N_2(g) stream at 173 ± 1 K. A total of 9867 reflections were collected, of which 3429 were unique. A disordered $[PF_6]^-$ anion required modeling in three different orientations. Final least-squares refinement of 242 parameters and 3203 data resulted in residuals of R1 = 0.0617 and wR2 = 0.1700. The goodness-of-fit index was 1.078, and the highest peak in the final difference map was 0.952 e$^-$/Å^{-3}.

$[Rh_2(O_2CCH_3)_2(pynp)_2][BF_4]_2\cdot C_7H_8$ (3). X-ray quality crystals were obtained by slow diffusion of an acetonitrile solution of the title compound into toluene. A red, rectangular crystal of dimensions 0.05 × 0.06 × 0.15 mm^3 was covered with silicone grease, secured on the tip of a glass fiber, and cooled to 173 ± 2 K. The data could not be treated directly because of a twinning problem, and so, the TWINNING package[20] was used instead. Two solutions had similar cell parameters but different orientation matrices. TWINDX[20] yielded two cells with a rotational angle of ∼37° between them. Data integration was carried out separately on the two orientation matrices. The data sets were corrected for inhomogeneity, decay, and adsorption with the SADABS program and then merged by XPREP and truncated to a resolution of 0.95 Å (2θ = 47°) to suppress effects of solvent and anion disorder. A total of 7670 reflections was collected, of which 3203 were unique. The structure was solved by direct methods with the SIR97 program[21] which led to the location of the main structure fragment and the disordered toluene. In the later stages of refinement, two disordered $[BF_4]^-$ anions were located near 2-fold symmetry elements and were modeled at 50% occupancy. Final least-squares refinement of 294 parameters and 1840 data resulted in residuals of R1 = 0.1062 and wR2 = 0.2365 and a goodness-of-fit of 1.117. A final difference Fourier map revealed the highest peak to be 0.952 e$^-$/Å^3.

$[Rh_2(O_2CCH_3)_2(pynp)_2(CH_3CN)_2][BF_4][PF_6]\cdot 2CH_3CN$ (4). Crystals suitable for X-ray crystallographic studies were obtained by slow diffusion of a solution of $[Rh_2(O_2CCH_3)_2(CH_3CN)_6][BF_4]_2$ in acetonitrile layered over a solution of pynp in dichloromethane. A pale red prism of dimensions 0.15 × 0.05 × 0.1 mm^3 was covered with silicone grease, mounted on the tip of a glass fiber, and placed in a N_2(g) cold stream at 173 ± 2 K. A total of 23918 reflections were collected, of which 9970 were unique. Final least-squares refinement of 598 parameters and 5987 reflections resulted in residuals of wR1 = 0.0678 and wR2 = 0.1642 and a goodness-of-fit of 0.980. A final difference Fourier map revealed the highest peak to be 2.209 e$^-$/Å^3 which is associated with a disordered $[PF_6]^-$.

Results and Discussion

Synthesis of Compounds $[M_2(O_2CCH_3)_2(pynp)]^{2+}$ (M = Mo^{II}, Ru^{II}, Rh^{II}). Reactions of pynp with $[Mo_2^{II,II}(O_2CCH_3)(CH_3CN)_6][BF_4]_2$,[11] $[Rh_2^{II,II}(O_2CCH_3)_2(CH_3CN)_6][BF_4]_2$,[12] and $[Ru_2^{II,III}(O_2CCH_3)_4Cl]$[10] carried out in a 1:2 metal/ligand ratio (eqs 2, 3) proceed instantaneously as judged by the fact that color changes occur within minutes of mixing the reagents. The replacement of the six acetonitrile molecules in the starting materials $[M_2(O_2CCH_3)_2(CH_3CN)_6][BF_4]_2$ to yield $[M_2(O_2CCH_3)_2(pynp)_2][BF_4]_2$ (M = Mo, Rh) occurs in methanol, ethanol, and acetone regardless of different ligand/metal ratios or reaction temperatures. The chemistry of $[Rh_2(O_2CCH_3)_2(CH_3CN)_6][BF_4]_2$ with pynp also involves the formation of a minor side product identified as $[Rh_2(O_2CCH_3)_2(pynp)_2(CH_3CN)_2][BF_4][PF_6]\cdot 2CH_3CN$ (**4**) by

(20) Sparks, R. A. *TWINNING (TWINDX, TWUTIL, TWROT and TWHKL), Program for processing twinned data*; Bruker AXS Instrument: Madison, WI.

(21) Altomare, A.; Burla, M. C.; Camalli, M.; Cascarano, G. L.; Giacovazzo, C.; Guagliardi, A.; Moliterni, A. G. G.; Polidori, G.; Spagna, R. *J. Appl. Crystallogr.* **1999**, *32*, 115.

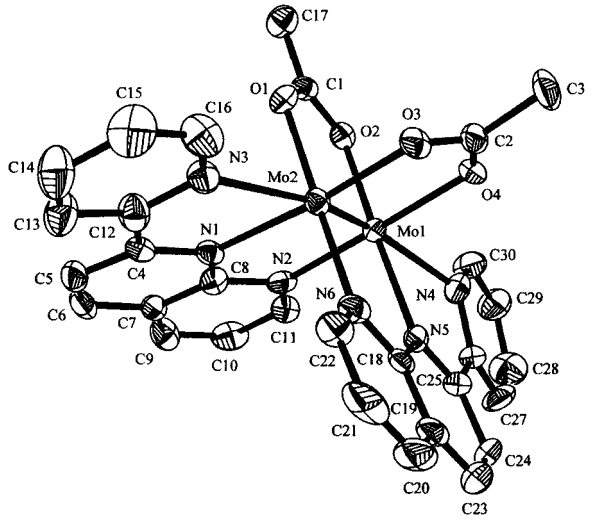

Figure 2. Thermal ellipsoid plot of the cation in $[Mo_2(O_2CCH_3)_2(pynp)_2][BF_4]_2 \cdot CH_3CN$ (**1**) at the 50% probability level. Hydrogens have been omitted for the sake of clarity.

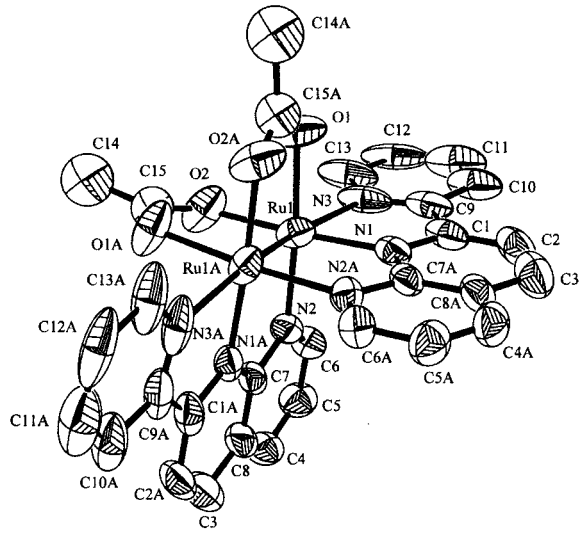

Figure 3. Thermal ellipsoid plot of the cation in $[Ru_2(O_2CCH_3)_2(pynp)_2][PF_6]_2 \cdot CH_3OH$ (**2**) at the 50% probability level. Hydrogen atoms have been omitted for the sake clarity.

single-crystal X-ray methods. The synthesis of the dinuclear $Ru_2^{II,II}$ complex is best performed in alcohols, as reactions performed in acetonitrile and acetone lead to much lower yields. Moreover, the diruthenium reaction involves a loss of two acetate ligands and a reduction from $Ru_2^{II,III}$ to $Ru_2^{II,II}$.

$$[M_2(OAc)_2(CH_3CN)_6][BF_4]_2 + 2pynp \xrightarrow{CH_3CN} [M_2(OAc)_2(pynp)_2][BF_4]_2 \quad (2)$$

M = (a) Mo^{2+}, (b) Rh^{2+} yield: a = 75%, b = 70%

$$[Ru_2(OAc)_4]Cl + 2pynp \xrightarrow[[n\text{-}Bu_4N][PF_6]]{CH_3OH} [Ru_2(OAc)_2(pynp)_2][PF_6]_2 \quad (3)$$

yield: 60%

X-ray Crystallographic Studies. The molecular structures of the dinuclear cations for compounds **1**−**3** are essentially identical (Figures 2−4, Tables 2−4). The compounds consist of a dimetal unit spanned by two cis, tridentate pynp ligands in addition to two bridging acetate ligands. This series of compounds is convenient for studying the effect of a π donor ligand such as pynp on the electronic properties of related M−M bonded compounds. One interesting aspect to consider is the axial interaction between the metal and the nitrogen donor of the pyridyl unit. The pseudoaxial pyridine interaction is relatively long in all three cases, with M−N distances ranging from 2.204(4) to 2.439(8) Å and M−M−N_{ax} angles in the range 159.01[2]−169.6(3)°. $[Mo_2(O_2CCH_3)_2(pynp)_2][BF_4]_2 \cdot 3CH_3CN$ (**1**) exhibits the longest axial M−N distance of 2.439[8] Å, as expected for a $Mo_2^{II,II}$ quadruply bonded complex.[22] In the case of $[Ru_2(O_2CCH_3)_2(pynp)_2][PF_6]_2 \cdot 2CH_3OH$ (**2**), the axial interaction Ru(1)−N(3) = 2.237(7) Å is consistent with the fact that this species is a doubly bonded compound. Finally, $[Rh_2(O_2CCH_3)_2(pynp)_2][BF_4]_2 \cdot C_7H_8$ (**3**) exhibits the shortest axial interaction, 2.204(4) Å (Rh(1)−N(3)), as expected for the compound with the weakest M−M bond trans influence.[22]

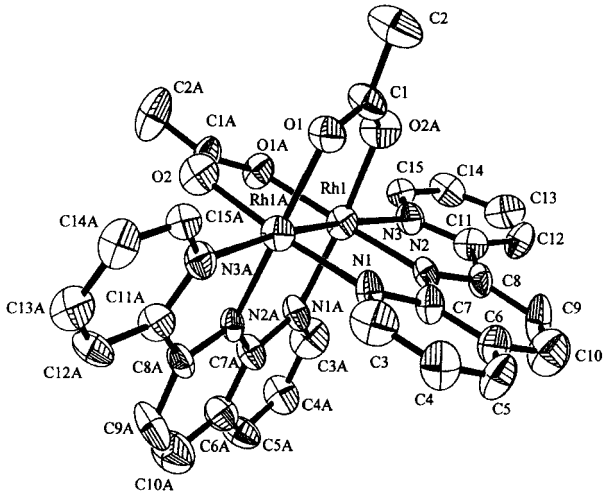

Figure 4. Thermal ellipsoid plot of the cation in $[Rh_2(O_2CCH_3)_2(pynp)_2][BF_4]_2 \cdot C_7H_8$ (**3**) at the 50% probability level. Hydrogen atoms have been omitted for the sake of clarity.

The strength of the axial M−L interaction is reflected in the M−M distance, a point that is nicely illustrated in this series of compounds. The quadruply bonded compound $[Mo_2(O_2CCH_3)_2(pynp)_2][BF_4]_2 \cdot 3CH_3CN$ (**1**) exhibits a M−M bond distance of 2.124(1) Å, whereas the reported M−M distance for the parent molecule $Mo_2(O_2CCH_3)_4$ is 2.0934(8) Å.[23] The lengthening of the metal−metal bond by 0.03 Å is attributed primarily to the axial interaction. The diruthenium compound in this series, namely $[Ru_2(O_2CCH_3)_2(pynp)_2][PF_6]_2 \cdot 2CH_3OH$ (**2**), exhibits a Ru−Ru distance of 2.298(1) Å, which is slightly longer than the corresponding distances in $Ru_2(O_2CCH_3)_4(THF)_2$ and $Ru_2(O_2CCH_3)_4(H_2O)_2$, which are 2.261(3) and 2.265(3) Å, respectively.[24] This lengthening is attributed to the fact that the pyridyl ring is a better axial donor than is THF or H_2O. Finally, in $[Rh_2(O_2CCH_3)_2(pynp)_2]$-

(22) Cotton, F. A.; Walton, A. R. *Multiple Bonds Between Metal Atoms*; Clarendon Press: Oxford, 1993.

(23) Cotton, F. A.; Mester, Z. C.; Webb, T. R. *Acta Crystallogr.* **1974**, *B30*, 2768.

Table 2. Selected Bond Distances (Å) and Angles (deg) for $[Mo_2(O_2CCH_3)_2(pynp)_2][BF_4]_2 \cdot 3CH_3CN$ (**1**)

Mo1−O3	2.088(6)	Mo2−O2	2.092(6)
Mo1−O1	2.114(6)	Mo2−O4	2.150(6)
Mo1−Mo2	2.124(1)	Mo2−N2	2.165(8)
Mo1−N6	2.184(8)	Mo2−N5	2.245(7)
Mo1−N1	2.251(7)	Mo2−N4	2.450(8)
Mo1−N3	2.429(8)		
O3−Mo1−O1	88.4(2)	O2−Mo2−Mo1	93.33(18)
O3−Mo1−Mo2	93.5(2)	O2−Mo2−O4	88.0(2)
O1−Mo1−Mo2	89.7(2)	Mo1−Mo2−O4	89.20(19)
O3−Mo1−N6	88.1(3)	O2−Mo2−N2	88.5(3)
O1−Mo1−N6	174.3(3)	Mo1−Mo2−N2	94.7(2)
Mo2−Mo1−N6	95.1(2)	O4−Mo2−N2	174.9(3)
O3−Mo1−N1	174.7(3)	O2−Mo2−N5	175.9(3)
O1−Mo1−N1	87.6(3)	Mo1−Mo2−N5	90.7(2)
Mo2−Mo1−N1	90.1(2)	O4−Mo2−N5	91.2(3)
N6−Mo1−N1	95.5(3)	N2−Mo2−N5	92.0(3)
O3−Mo1−N3	106.1(3)	O2−Mo2−N4	106.6(3)
O1−Mo1−N3	84.3(3)	Mo−Mo2−N4	158.7(2)
Mo2−Mo1−N3	159.3(2)	O4−Mo2−N4	84.1(3)
N6−Mo1−N3	92.2(3)	N2−Mo2−N4	93.4(3)
N1−Mo1−N3	69.9(3)	N5−Mo2−N4	69.3(3)

Table 3. Selected Bond Distances (Å) and Angles (deg) for $[Ru_2(O_2CCH_3)_2(pynp)_2][PF_6]_2 \cdot 2CH_3OH$ (**2**)

Ru1−Ru1	2.298(1)	Ru1−N1	2.071(5)
Ru1−O2	2.054(5)	Ru1−O1	2.089(5)
Ru1−N2	2.072(5)	Ru1−N3	2.237(7)
O2−Ru1−N2	90.2(2)	O1−Ru1−N3	87.6(2)
O2−Ru1−N1	176.7(2)	O2−Ru1−Ru1	91.22(14)
N2−Ru1−N1	93.0(2)	N2−Ru1−Ru1	91.2(2)
N2−Ru1−O1	175.6(2)	N1−Ru1−Ru1	89.4(2)
N1−Ru1−O1	90.9(2)	O1−Ru1−Ru1	86.91(14)
N2−Ru1−N3	95.3(2)	N3−Ru1−Ru1	163.7(2)

Table 4. Selected Bond Distances (Å) and Angles (deg) for $[Rh_2(O_2CCH_3)_2(pynp)_2][BF_4]_2 \cdot C_7H_8$ (**3**)

Rh1−Rh1	2.408(2)	Rh1−N1	2.045(12)
Rh1−N2	1.985(12)	Rh1−O1	2.051(11)
Rh1−O2	2.036(11)	Rh1−N3	2.204(11)
N2−Rh1−O2	90.2(5)	O2−Rh1−N3	90.4(4)
N2−Rh1−N1	92.0(5)	N1−Rh1−N3	95.6(4)
O2−Rh1−N1	173.8(4)	O1−Rh1−N3	101.7(4)
N2−Rh1−O1	178.7(4)	N2−Rh1−Rh1	91.1(3)
O2−Rh1−O1	88.6(4)	O2−Rh1−Rh1	86.9(2)
N1−Rh−O1	89.2(4)	N1−Rh1−Rh1	87.3(3)
N2−Rh1−N3	78.9(4)	O1−Rh1−Rh1	88.3(2)

$[BF_4]_2 \cdot C_7H_8$ (**3**), the Rh−Rh distance is 2.408(2) Å, which is well within the expected range for a Rh−Rh single bond.[18] This distance is 0.04 Å longer than the corresponding distance in $Rh_2(O_2CC_3H_7)_4$,[25] which is the only dirhodium tetracarboxylate compound without axial coordination to be reported to our knowledge. The lengthening of the M−M bond is due to the donation of the pyridyl moiety into the σ^* antibonding orbital of the $[Rh_2]^{4+}$ unit.

The $M-N_{eq}$ interactions with the naphthyridine bridges are considerably weaker than the $M-N_{ax}$ interactions by comparison, and they weaken as the radius of the metal ion decreases. Accordingly, the Mo−N distances are the longest: $Mo-N_{av} = 2.211(8)$ Å, followed by $Ru-N_{av} = 2.072(5)$ Å, and finally, $Rh-N_{av} = 2.018(4)$ Å.

Table 5. Selected Bond Distances (Å) and Angles (deg) for $[Rh_2(O_2CCH_3)_2(pynp)_2(CH_3CN)_2][BF_4][PF_6] \cdot 2CH_3CN$ (**4**)

Rh1−Rh2	2.3555(11)	Rh1−N4	2.158(5)
Rh1−N8	2.034(6)	Rh1−O3	2.176(5)
Rh1−O1	2.084(5)	Rh2−N3	1.997(5)
Rh1−N1	2.134(6)		
N8−Rh1−O1	178.0(2)	N1−Rh1−O3	174.2(2)
N8−Rh1−N1	95.6(2)	N4−Rh1−O3	94.8(2)
O1−Rh1−N1	85.1(2)	N8−Rh1−Rh2	93.27(14)
N8−Rh1−N4	95.5(2)	O1−Rh1−Rh2	88.46(12)
O1−Rh1−N4	82.7(2)	N1−Rh1−Rh2	97.86(14)
N1−Rh1−N4	90.9(2)	N4−Rh1−Rh2	167.0(2)
N8−Rh1−O3	85.3(2)	O3−Rh1−Rh2	76.30(11)
O1−Rh1−O3	94.2(2)		

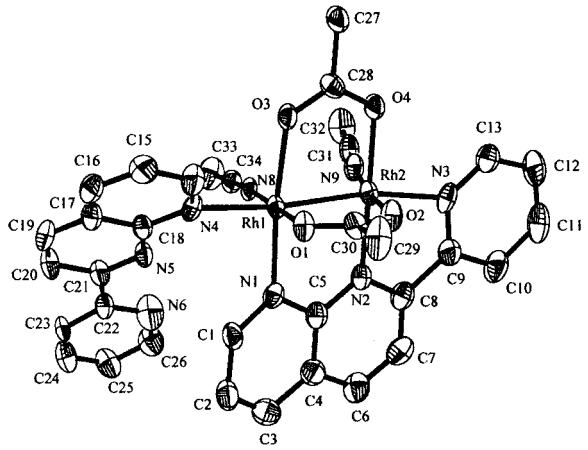

Figure 5. Thermal ellipsoid plot of the cation in $[Rh_2(O_2CCH_3)_2(pynp)_2(CH_3CN)_2][BF_4][PF_6]_2 \cdot CH_3CN$ (**4**) at the 50% probability level. Hydrogen atoms have been omitted for the sake of clarity.

As noted earlier, in addition to $[Rh_2(O_2CCH_3)_2(pynp)_2][BF_4]_2$ (**3**), a minor by-product was isolated and determined to be $[Rh_2(O_2CCH_3)_2(pynp)_2(CH_3CN)_2][BF_4][PF_6] \cdot 2CH_3CN$ (**4**) by X-ray crystallography (Table 5). In this compound, the dirhodium unit possesses one pynp ligand coordinated in the usual tridentate fashion and a second pynp ligand that acts as a monodentate axial ligand to an axial position through one of the N atoms of the naphthyridine unit (Figure 5). Besides the four oxygen atoms of the trans acetate ligands, the two remaining equatorial positions are occupied by acetonitrile molecules. The pseudoaxial distance (Rh(1)−N(4)) between the η^1-pynp ligand and the metal center is 2.158(5) Å, which is 0.16 Å larger than the Rh−pyridyl interaction Rh(2)−N(3), 1.997(5) Å. The weaker Rh−N interaction is presumably due to the weaker donor character of the naphthyridine nitrogen atom compared to that of the pyridine nitrogen unit.

Electronic Spectroscopy. The electronic spectra for the three compounds in the series $[M_2(O_2CCH_3)_2(pynp)_2][BF_4]_2$ were recorded in acetonitrile in the range 800−200 nm (Table 6). The spectrum for $[Mo_2(O_2CCH_3)_2(pynp)_2][BF_4]_2$ (**1**) exhibits an electronic transition in the visible region at 432 nm which is a characteristic energy for a $\delta \rightarrow d^*$ transition for a quadruply bonded $Mo_2^{II,II}$ complex.[26,27] The

(24) Lindsay, A. J.; Tooze, R. P.; Motevall, M.; Hursthousean, M. B.; Wilkinson, G. *J. Chem. Soc., Commun.* **1984**, 1383.
(25) Cotton, F. A.; Shiu, K. B. *Rev. Chim. Miner.* **1986**, *23*, 14.
(26) Trogler, W. C.; Gray, H. B. *Acc. Chem. Res.* **1978**, *11*, 232.
(27) Trogler, W. C.; Solomon, E. I.; Trajberg, I. B.; Ballhausen, C. J.; Gray, H. B. *Inorg. Chem.* **1977**, *16*, 828.

Table 6. UV−Vis Data for Compounds **1**−**3**

compound	λ_{max} (nm)	ϵ·(L·M^{-1} cm^{-1})
$[Mo_2(O_2CCH_3)_2(pynp)_2][BF_4]_2$ (**1**)	432	1.8×10^3
	857	4.8×10^2
$[Ru_2(O_2CCH_3)_2(pynp)_2][PF_6]_2$ (**2**)	327	3.4×10^4
	671	3.6×10^4
$[Rh_2(O_2CCH_3)_2(pynp)_2][BF_4]_2$ (**3**)	278	3.1×10^4
	355	8.7×10^3
	451	2.4×10^3

ϵ value of 1.8×10^3 L·M^{-1} cm^{-1} is uncharacteristically high, however, which is an indication of the involvement of ligand character.

The dinuclear ruthenium complex (**2**) exhibits electronic transitions located at 327 ($\epsilon = 3.4 \times 10^4$ L·M^{-1} cm^{-1}) and 671 nm ($\epsilon = 3.6 \times 10^4$ L·M^{-1} cm^{-1}), and the dirhodium compound (**3**) displays transitions located at 278, 355, and 451 nm with ϵ values of 3.1×10^4, 8.7×10^3, and 2.4×10^3 L·M^{-1} cm^{-1}, respectively.

These optical spectra indicate that the new compounds exhibit quite different electronic properties than those of the parent tetracarboxylate species. Electronic transitions for $[Mo_2(O_2CCH_3)_4]$ are located at 435 nm ($\epsilon \approx 10^2$ L·M^{-1} cm^{-1}),[27] for $[Rh_2(O_2CCH_3)_4]L_2$ at $\lambda_{max} = 552$ ($\epsilon \approx 2 \times 10^2$ L·M^{-1} cm^{-1}) and 437 nm ($\epsilon \approx 1 \times 10^2$ L·M^{-1} cm^{-1}),[28] and finally, for $[Ru_2II,II(O_2CCH_3)_4]$ at $\lambda_{max} = 448$ nm ($\epsilon \approx 6 \times 10^2$ L·M^{-1} cm^{-1}).[22] Clearly, the presence of the two pynp ligands perturbs the electronic structure of the HOMO and/or LUMO levels. The nature of the HOMO and LUMO levels was probed by theoretical calculations (vide supra).

^{1}H NMR Spectroscopy. ^{1}H NMR spectroscopic studies of the two diamagnetic compounds $[Mo_2(O_2CCH_3)_2(pynp)_2][BF_4]_2$ (**1**) and $[Rh_2(O_2CCH_3)_2(pynp)_2][BF_4]_2$ (**3**) in CD_3CN support the existence of the intact molecular cations in solution. The ^{1}H NMR spectrum of **1** displays an upfield singlet at $\delta = 2.65$ ppm for the acetate CH_3 groups and seven resonances between 7.5 and 9.0 ppm for the aromatic pynp protons. Compound **3** exhibits a similar pattern, with an upfield singlet located at $\delta = 2.25$ ppm and aromatic resonances in the range 7.5−9.7 ppm. The presence of only one acetate environment in each case and the 1:1 integration of acetate/pynp ligands is in accord with the solid-state structure.

Cyclic Voltammetric Studies. Electrochemical studies of compounds **1**−**3** were performed in acetonitrile solution (Figure 6). The cyclic voltammogram of $[Mo_2(O_2CCH_3)_2(CH_3CN)_6][BF_4]_2$ exhibits four reversible reduction couples located at $E_{1/2}^{(1)} = -0.43$ V, $E_{1/2}^{(2)} = -0.67$ V, $E_{1/2}^{(3)} = -1.34$ V, and $E_{1/2}^{(4)} = -1.66$ V (Figure 6). In addition, an irreversible metal-based oxidation occurs at $E_{pa} = 0.86$ V. While the oxidation is metal-based, the reductions are mainly ligand-based, as judged by the fact that free pynp exhibits a 2e$^-$ reduction at a potential of $E_{1/2} = -1.62$ V.

When the pynp ligands are coordinated to the dimetal unit, the 2e$^-$ processes corresponding to each of the two ligands are separated into two 1e$^-$ processes, an indication that the mixed valence 1e$^-$ intermediates are stabilized by delocalized

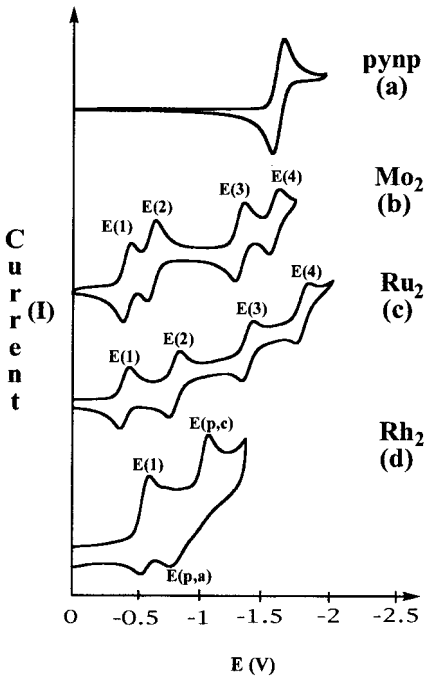

Figure 6. Cyclic voltammograms for the free pynp ligand and compounds **1**−**3** in 0.1 M [*n*-Bu$_4$N][PF$_6$]/CH$_3$CN at a Pt disk electrode versus Ag/AgCl.

Scheme 1

$$[M_2(O_2CCH_3)_2(pynp)_2]^{2+} + [M_2(O_2CCH_3)_2(pynp)_2] \underset{-e^-}{\overset{+e^-}{\rightleftharpoons}} 2[M_2(O_2CCH_3)_2(pynp)_2]^+$$

K_c for Mo = 1.2 x 10^4; K_c for Ru = 3.9 x 10^6 (a)

$$[M_2(O_2CCH_3)_2(pynp)_2] + [M_2(O_2CCH_3)_2(pynp)_2]^{2-} \underset{-e^-}{\overset{+e^-}{\rightleftharpoons}} 2[M_2(O_2CCH_3)_2(pynp)_2]^-$$

K_c for Mo = 2.7 x 10^5; K_c for Ru = 2.7 x 10^7 (b)

bonding. For $[Mo_2(O_2CCH_3)_2(CH_3CN)_6][BF_4]_2$, the second 1e$^-$ reduction occurs at a potential that is 240 mV more negative than the first 1e$^-$ couple. This value reflects the degree of electronic communication between the ligands and can be related to a comproportionation constant, $K_c = 1.2 \times 10^4$, for the reaction shown in Scheme 1a. This equilibrium constant is in the range of Class II weakly coupled systems according to the Robin−Day classification for electron delocalization.[29] Likewise, the second set of 1e$^-$ reductions is also weakly coupled as judged by the fact that the fourth 1e$^-$ reduction occurs at a potential which is 320 mV higher than that of the third reduction process (K_c value of 2.70×10^5) (Scheme 1b).

Similar electrochemical behavior was observed for $[Ru_2(O_2CCH_3)_2(pynp)_2][PF_6]_2$, which exhibits four reversible 1e$^-$ ligand-based reductions; these are located at $E_{1/2}^{(1)} = -0.43$ V, $E_{1/2}^{(2)} = -0.82$ V, $E_{1/2}^{(3)} = -1.40$ V, and $E_{1/2}^{(4)} = -1.84$ V. A reversible oxidation couple at $E_{1/2} = +0.85$ V is assigned to an oxidation from $Ru_2^{II,II}$ to $Ru_2^{II,III}$. As compared to the Mo derivative the separations for the 2e$^-$ processes in this compound are greater. Specifically, the second 1e$^-$ reduction is shifted to a more negative potential by 390 mV relative to the first one, which is a K_c value of 3.9×10^6 or

(28) Johnson, S. A.; Hunt, H. R.; Neumann, H. M. *Inorg. Chem.* **1963**, *2*, 960.

(29) Robin, M. B.; Day, P. *Adv. Inorg. Chem. Radiochem.* **1967**, *10*, 247.

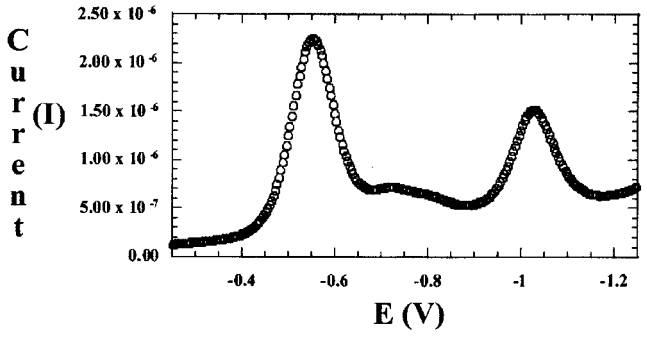

Figure 7. Differential pulse voltammogram of $[Rh_2(O_2CCH_3)_2(pynp)_2][BF_4]_2$ in 0.1 M $[n\text{-}Bu_4N][PF_6]/CH_3CN$ at a Pt disk electrode versus Ag/AgCl.

Class III behavior typical of completely delocalized electronic systems. In a similar vein, the third and fourth reductions occur with a separation of 420 mV, which leads to a calculated K_c value of 2.7×10^7.

In contrast to the previous two cases, $[Rh_2(O_2CCH_3)_2(pynp)_2]^{2+}$ exhibits only two reduction features in the cyclic voltammogram; the first one is quasireversible with $E_{1/2}^{(1)} = -0.59$ V, while the second one is irreversible and shows $E_{p,c}^{(2)} = -1.10$ V with an associated returning wave at $E_{p,a}^{(2)} = -0.80$ V (Figure 6c). The first reduction process is associated with a $2e^-$ process, with almost negligible splitting into the individual $1e^-$ proccesses. The second reduction is a one-electron process as determined by coulometry and differential pulse voltammetry (Figure 7).

Theoretical Results. To gain insight into the electronic structure of the compounds in the series $[M_2(O_2CCH_3)_2(pynp)_2]^{2+}$ (M = Mo, Ru, Rh), single point energy calculations were performed at the B3LYP level of theory for three redox forms of the compounds, namely $[M_2(O_2CCH_3)_2(pynp)_2]^{2+}$, $M_2(O_2CCH_3)_2(pynp)_2$, and $[M_2(O_2CCH_3)_2(pynp)_2]^{2-}$. In the case of the Ru_2 compounds, calculations were also performed on $[Ru_2(O_2CCH_3)_2(pynp)_2]^+$ and $[Ru_2(O_2CCH_3)_2(pynp)_2]^-$. Analyses of the calculated orbital occupancies for the dications $[Mo_2(O_2CCH_3)_2(pynp)_2]^{2+}$, $[Rh_2(O_2CCH_3)_2(pynp)_2]^{2+}$, and $[Ru_2(O_2CCH_3)_2(pynp)_2]^{2+}$ support the electronic configurations $\sigma^2\pi^4\delta^2$, $\sigma^2\pi^4\delta^2\delta^{*2}\pi^{*4}$, and $\sigma^2\pi^4\delta^2\delta^{*2}\pi^{*2}$, respectively. To simplify the discussion, the abbreviations $[M_2]^{2+}$, $[M_2]^+$, $[M_2]^0$, $[M_2]^-$, and $[M_2]^{2-}$ will be used to designate the original compounds ($[M_2]^{2+}$) and the various reduction products.

Correlation with Electronic Transitions. The calculated energy differences between the highest occupied molecular orbital (HOMO) and lowest unoccupied molecular orbital (LUMO) levels for each of the three new compounds from DFT calculations were compared to the aforementioned spectroscopic data (vide infra). In all cases, the lowest energy transition is one that involves metal-to-ligand charge-transfer character (MLCT), which is in accord with the high ϵ values observed for these transitions.[30] The calculated energy differences between the LUMO and HOMO levels of the dicationic species $[M_2]^{2+}$ correspond to the lowest energy transitions observed in the UV−visible spectra for these species (Figure 8). In the case of $[Mo_2]^{2+}$ (**1**), the lowest energy transition is a predictable $\delta \rightarrow \delta^*$ transition, with a calculated ($E_{LUMO} - E_{HOMO}$) energy gap of 33.6 kcal/mol as compared to the experimental value of 33.3 kcal/mol. The extinction coefficient for this transition ($\epsilon = 4.75 \times 10^2$ L M^{-1} cm^{-1}) is an order of magnitude greater than those reported for a typical $\delta \rightarrow \delta^*$ transition.[22] The calculation indicates that the LUMO involved in the first electronic transition of $[Mo_2]^{2+}$ contains much greater ligand character than the HOMO (Table 7). These results indicate that the lowest energy transition involves a metal-to-ligand charge transfer (MLCT) which explains the larger than expected extinction coefficients.

The lowest energy transition for $[Rh_2]^{2+}$ was calculated to be from a metal-based $d\pi^*$ orbital to a ligand-based $p\pi^*$ orbital ($M_{\pi^*} \rightarrow L_{\pi^*}$) with a value of 63.9 kcal/mol, in good agreement with the experimental value of 63.4 kcal/mol (Figure 8). The observed ϵ value of 2.4×10^3 L M^{-1} cm^{-1} for $[Rh_2]^{2+}$ is an order of magnitude greater than the ϵ value observed for the first transition of $[Mo_2]^{2+}$. This finding is consistent with an increase in the ligand character for the orbitals of $[Rh_2]^{2+}$ involved in the transition as compared to the $[Mo_2]^{2+}$ case (Table 7).

Finally, the lowest energy transition for $[Ru_2]^{2+}$ was calculated to be a $M_{\pi^*} \rightarrow L_{\pi^*}$ transition (MLCT) with an energy of 59.3 kcal/mol. The experimental value for this transition is 42.6 kcal/mol, which is in reasonable agreement with the calculations (Figure 8). The MLCT character for $[Ru_2]^{2+}$ is calculated to be close to that of $[Rh_2]^{2+}$, which is consistent with the similar extinction coefficient for $[Ru_2]^{2+}$ versus $[Rh_2]^{2+}$ ($\epsilon = 3.4 \times 10^4$ and 3.1×10^4 L M^{-1} cm^{-1}, respectively). An overestimation of the excitation energy is not entirely unexpected for this type of calculation, as the correlation energy of the excitation is not included, but it is a little surprising, given the close agreement of the calculated and experimental results for the other two compounds. It should be noted that the dication of $[Ru_2]^{2+}$ requires an unrestricted open shell calculation with two unpaired electrons ($S = 1$ with the α and β orbitals being independently optimized), whereas both $[Mo_2]^{2+}$ and $[Rh_2]^{2+}$ involve closed shell calculations.

Correlation with Electrochemistry. To study the electronic properties of $[Ru_2(O_2CCH_3)_2(pynp)_2]^{2+}$, open shell calculations are unavoidable because the ground state is a triplet ($S = 1$).[31] Therefore, B3LYP single point energy calculations were performed for all five different oxidation states of the diruthenium compounds observed in the electrochemical experiments, viz., $[Ru_2(O_2CCH_3)_2(pynp)_2]^{(2+/1+/0/1-/2-)}$. A single point energy calculation was performed on both the singlet ($S = 0$) and triplet ($S = 1$) states of $[Ru_2(O_2CCH_3)_2(pynp)_2]^{2+}$, and the triplet was found to be 35.4 kcal/mol lower in energy, in agreement with the magnetic measurements.[31]

(30) (a) Trogler, W. C.; Solomon, I.; Trabjerg, C. J.; Ballhausen, C. J.; Gray, H. B. *Inorg. Chem.* **1977**, *16*, 828. (b) Martin, D. S.; Newman, R. A.; Fanwick, P. E. *Inorg. Chem.* **1979**, *18*, 2511. (c) Miskowski, V. M.; Schaefer, B.; Sadeghi, B. D.; Santarsiero, B. D.; Gray, H. B. *Inorg. Chem.* **1984**, *23*, 1154. (d) Miskowski, V. M.; Loehr, T. M.; Gray, H. B. *Inorg. Chem.* **1987**, *26*, 1098. (e) Miskowski, V. M.; Gray, H. B. *Inorg. Chem.* **1988**, *27*, 2501. (f) Clark, R. J. H.; Ferris, L. T. H. *Inorg. Chem.* **1981**, *20*, 2759.

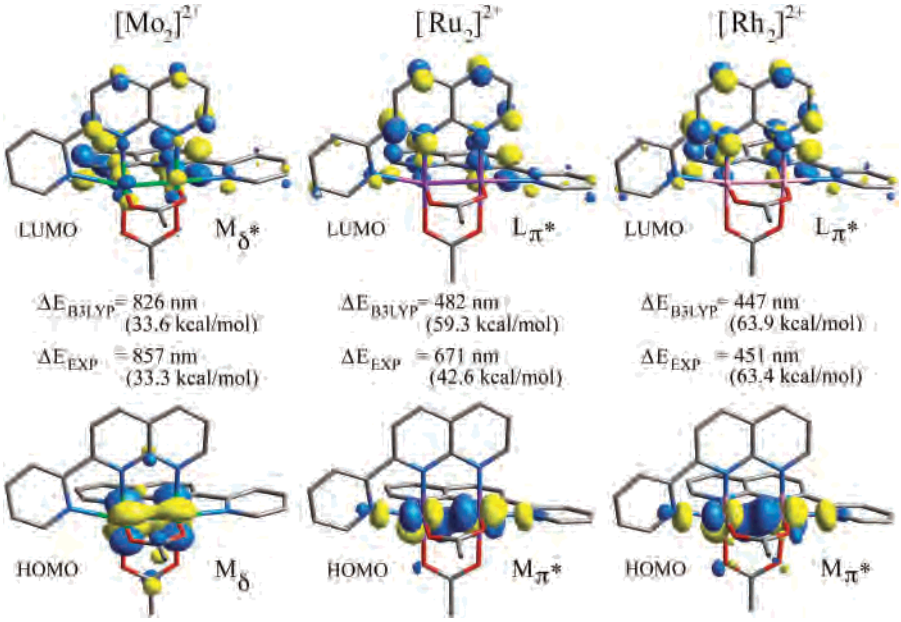

Figure 8. B3LYP calculated 0.05 isodensity surface of the HOMO and LUMO for $[M_2(O_2CCH_3)_2(pynp)_2]^{2+}$, where ΔE(B3LYP) is the calculated difference between the energy of the HOMO and LUMO and ΔE(EXP) is the experimentally determined excitation energy.

Table 7. Ratio of Metal to Ligand (M/L) and Ligand to Metal (L/M) Character of the Highest Occupied Molecular Orbital (HOMO) and the Lowest Unoccupied Molecular Orbital (LUMO) as Calculated at the B3LYP Level of Theory for the Dication $[M_2(O_2CCH_3)_2(pynp)_2]^{2+}$ (M = Mo^{2+}, Ru^{2+} and Rh^{2+}) of **1**, **2**, and **3**

	HOMO M/L	LUMO M/L	HOMO L/M	LUMO L/M
Mo(+2)	1.63	0.36	0.61	2.74
Ru(+2)[a]	1.53	0.01	0.65	9.87
Rh(+2)	1.33	0.09	0.75	11.5

[a] HOMO and LUMO for the α molecular orbitals.

The calculations were analyzed as discussed in the Experimental Section of the paper, and the NCOE values were compared to the electrochemical potentials for the reduction of the parent compound $[Ru_2]^{2+}$. The relevant orbital energies, their differences, and the NCOE values for compound **2** are listed in Table 8. The NCOE value for the $1e^-$ reduction of $[Ru_2]^{2+}$ was calculated to be 0.45, while the NCOE value for the $1e^-$ reduction of neutral compound $[Ru_2]^0$ was calculated to be 0.66. The NCOE value is proportional to the difference in the electrochemical potentials for the first and second reduction couples; these values indicate that the intermediate $[Ru_2]^-$ is more stabilized with respect to addition of the second $1e^-$ reduction than is $[Ru_2]^+$. Another way of stating this point is that the splitting of the potentials for the second $2e^-$ process should be greater than for the first one. To correlate this with the electrochemistry, we note that the cyclic voltammogram for $[Ru_2(O_2CCH_3)_2(pynp)_2][PF_6]_2$ exhibits a separation of $\Delta E_{1/2} = 390$mV for the $1e^-/2e^-$ reduction versus $\Delta E_{1/2} = 420$mV for the $3e^-/4e^-$; these values are consistent with the calculated larger splitting of the second $2e^-$ reduction.

We also observed that this trend is consistent if we calculate the NCOE values for a $2e^-$ reduction instead of a $1e^-$ reduction. The NCOE values for the $2e^-$ reduction of $[Ru_2]^{2+}$ and $[Ru_2]^0$ were calculated and found to be 0.70 and 0.88, respectively, in good agreement with the $1e^-$ calculations. On the basis of this result, we expect that the modeling of $2e^-$ reductions can also provide a qualitative description of the separation of the two $1e^-$ reduction potentials while decreasing the computational cost.

With the aforementioned results in hand, DFT single point energy calculations were performed only for the closed shell oxidation states of the Mo_2 and Rh_2 compounds, namely $[Mo_2]^{(2+/0/2-)}$ and $[Rh_2]^{(2+/0/2-)}$. In these cases, only $2e^-$ reductions were simulated, because $1e^-$ reductions lead to open shell species ($S = {}^1/_2$) which are harder to compute than the closed shell species. Following the trend observed for the $[Ru_2]^{2+}$ example, the calculated NCOE values should be proportional to the separation of the $1e^-$ reduction potentials in the cyclic voltammetry for this series of compounds. The orbital energies, their differences, and the NCOE for compounds **1** and **3** are listed in Tables 9 and 10. For $[Mo_2]^{2+}$, the NCOE value for the first $2e^-$ reduction is 0.59, and for the second $2e^-$ reduction, it is 0.73. These numbers are in good agreement with the observed cyclic voltammogram of $[Mo_2(O_2CCH_3)_2(pynp)_2][BF_4]_2$ which reveals splittings of $\Delta E_{1/2} = 240$ mV ($1e^-/2e^-$) and $\Delta E_{1/2} = 320$ mV ($3e^-/4e^-$), for the first and second $2e^-$ reductions, respectively. The second splitting is larger, in accord with

(31) SQUID measurements performed over the temperature range 2−300 K confirm the $S = 1$ ground state with a small paramagnetic impurity. The following equation was used to fit the data: $\chi = (2Ng_M^2\mu_B^2/3\kappa T)\{[e^{-x} + (2/x)(1 - e^{-x})]/(1 + 2e^{-x})\} + TIP + P/T$where $3x = D/\kappa T$ accounts for the zero field splitting and $g_M = 2$. These assignments were based on previous studies performed on $[Ru_2]^{II,II}$ systems. See for example: (a) Bonnet, L.; Cukiernik, F. D.; Maldivi, P.; Giroud-Godquin, A.-M.; Marchon, J.-C. *Chem. Mater.* **1994**, *6*, 31. (b) Maldavi, P.; Giroud-Godquin, A.-M.; Marchon, J.-C.; Guillon, D.; Skoulios, A. *Chem. Phys. Lett.* **1989**, *157*, 552. (c) Cogne, A.; Belorizky, J.; Laugier, J.; Rey, P. *Inorg. Chem.* **1994**, *33*, 3364. (d) Cotton, F. A.; Miskowski, V. M.; Zhong, B. *J. Am. Chem. Soc.* **1989**, *111*, 6177. (e) Miyasaka, H.; Campos-Fernández, C. S.; Clérac, R.; Dunbar, K. R. *Angew. Chem., Int. Ed.* **2000**, *39*, 3831. (f) Miyasaka, H.; Clérac, R.; Campos-Fernández, C.-S.; Dunbar, K. R. *Inorg. Chem.* **2001**, *40*, 1663.

Table 8. Normalized Change in Orbital Energies (NCOE) Values for the 1e$^-$ Reductions of $[Ru_2]^{2+}$ along with Molecular Orbital Energies (hartrees) for the Pertinent Molecular Orbitals in Triplet ($S = 1$) $[Ru_2]^{2+}$, **2**, Doublet ($S = {}^1/_2$) $\mathbf{2}^{(1+/1-)}$, and Singlet ($S = 0$) $\mathbf{2}^{(0/2-)}$

	C1	C2	C3	C4	ΔE^a	ΔE^b	ΔE^c	NCOE^d
$[Ru_2]^{2+}$	β_{HOMO}	β_{LUMO}	β_{LUMO+1}	β_{LUMO+2}	ΔE_1	ΔE_2	ΔE_3	
	−0.3921	−0.3110	−0.3041	−0.2991	0.081	0.088	0.005	
$[Ru_2]^{1+}$	β_{HOMO-1}	β_{HOMO}	β_{LUMO}	β_{LUMO+1}	ΔE_4	ΔE_5	ΔE_6	$\Delta_{1,4}$
	−0.2790	−0.2275	−0.1927	−0.1894	0.051	0.086	0.003	0.45
$[Ru_2]^0$	α,β_{HOMO-2}	α,β_{HOMO-1}	α,β_{HOMO}	α,β_{LUMO}	ΔE_7	ΔE_8	ΔE_9	$\Delta_{2,8}$
	−0.1558	−0.1307	−0.1136	−0.0747	0.025	0.042	0.039	0.70
$[Ru_2]^{1-}$	α_{HOMO-3}	α_{HOMO-2}	α_{HOMO-1}	α_{HOMO}	ΔE_{10}	ΔE_{11}	ΔE_{12}	$\Delta E_{9,12}$
	−0.0445	−0.0256	−0.0160	0.0035	0.019	0.028	0.020	0.66
$[Ru_2]^{2-}$	α_{HOMO-3}	α_{HOMO-2}	α_{HOMO-1}	α_{HOMO}	ΔE_{13}	ΔE_{14}	ΔE_{15}	$\Delta E_{9,15}$
	0.0749	0.1082	0.1119	0.1270	0.033	0.037	0.015	0.88

[a] ΔE_m = (orbital energy in column C2 − orbital energy in column C1). [b] ΔE_n = (orbital energy in column C3 − orbital energy in column C1). [c] ΔE_p = (orbital energy in column C4 − orbital energy in column C3). [d] $\Delta_{x,y} = (\Delta E_x - \Delta E_y)/[(1/2)(\Delta E_x + \Delta E_y)]$.

Table 9. Normalized Change in Orbital Energies (NCOE) Values for 2e$^-$ Reductions of $[Mo_2]^{2+}$ along with Molecular Orbital Energies (hartrees) for the Pertinent Molecular Orbitals in Singlet ($S = 0$) $[Mo_2]^{(2+/0/2-)}$ (**1**)

	C1	C2	C3	ΔE^a	ΔE^b	NCOE^c
$[Mo_2]^{2+}$	HOMO	LUMO	LUMO+1	ΔE_1	ΔE_3	
	−0.3745	−0.3193	−0.3042	0.055	0.015	
$[Mo_2]^0$	HOMO−1	HOMO	LUMO	ΔE_3	ΔE_4	$\Delta_{1,3}$
	−0.1447	−0.1148	−0.0807	0.030	0.034	0.59
$[Mo_2]^{2-}$	HOMO−2	HOMO−1	HOMO	ΔE_5	ΔE_6	$\Delta_{4,6}$
	0.0713	0.1030	0.1189	0.032	0.016	0.73

[a] ΔE_n = (orbital energy in column C2 − orbital energy in column C1). [b] ΔE_m = (orbital energy in column C3 − orbital energy in column C2). [c] $\Delta_{x,y} = (\Delta E_x - \Delta E_y)/[(1/2)(\Delta E_x + \Delta E_y)]$.

Table 10. Normalized Change in Orbital Energies (NCOE) Values for 2e$^-$ Reductions of $[Rh_2]^{2+}$ along with Molecular Orbital Energies (hartrees) for the Pertinent Molecular Orbitals in Singlet ($S = 0$) $[Rh_2]^{(2+/0/2-)}$ (**1**)

	C1	C2	C3	ΔE^a	ΔE^b	NCOE^c
$[Rh_2]^{2+}$	HOMO	LUMO	LUMO+1	ΔE_1	ΔE_3	
	−0.4109	−0.3090	−0.3062	0.103	0.003	
$[Rh_2]^0$	HOMO−1	HOMO	LUMO	ΔE_3	ΔE_4	$\Delta_{1,3}$
	−0.1870	−0.1003	−0.0791	0.087	0.021	0.16
$[Rh_2]^{2-}$	HOMO−2	HOMO−1	HOMO	ΔE_5	ΔE_6	$\Delta_{4,6}$
	0.0435	0.1210	0.1223	0.078	0.001	1.77

[a] ΔE_n = (orbital energy in column C2 − orbital energy in column C1). [b] ΔE_m = (orbital energy in column C3 − orbital energy in column C2). [c] $\Delta_{x,y} = (\Delta E_x - \Delta E_y)/[(1/2)(\Delta E_x + \Delta E_y)]$.

the larger NCOE value for the second 2e$^-$ reduction versus the first 2e$^-$ reduction. In addition, the calculated NCOE values for the 2e$^-$ processes of $[Mo_2]^{2+}$ are smaller than the corresponding NCOE values for the 2e$^-$ reductions of $[Ru_2]^{2+}$, which also agrees with the smaller differences in potentials observed in the cyclic voltammetry experiments.

Finally, the NCOE values for $[Rh_2]^{2+}$ are 0.16 and 1.77 for the first and second 2e$^-$ reductions, respectively. As previously mentioned, the cyclic voltammogram for $[Rh_2]^{2+}$ is distinct from the behavior of $[Mo_2]^{2+}$ and $[Ru_2]^{2+}$. The calculated NCOE value for the 2e$^-$ reduction of $[Rh_2(O_2CCH_3)_2(pynp)_2][BF_4]_2$ is much smaller than the NCOE values calculated for the $[Mo_2]^{2+}$ and $[Ru_2]^{2+}$ analogues. This is entirely consistent with the fact that the first two 1e$^-$ reductions occur at nearly the same potential in the electrochemical data. The NCOE value of 1.77 calculated for the second 2e$^-$ process for $[Rh_2]^{2+}$ indicates that the splitting of the 1e$^-$ reduction potentials in this case should be extremely large (Table 10). Indeed, a differential pulse voltammetry (DPV) experiment performed on $[Rh_2(O_2CCH_3)_2(pynp)_2][BF_4]_2$ revealed that the first reversible process is a 2e$^-$ reduction, whereas the second quasireversible couple is only a 1e$^-$ reduction (Figure 7), in accord with the calculated NCOE values. The orbital occupation for the neutral species $Rh_2(O_2CCH_3)_2(pynp)_2$ is calculated to be $\sigma^2\pi^4\delta^2\delta^{*2}\pi^{*4}L(\pi^{*2})$, and the LUMO involves an antibonding interaction of the metal-δ^* with a ligand-π^* orbital. We note that the electrochemical processes for this complex are not perfectly reversible and that the second reduction is only a 1e$^-$ reduction, which suggests that the neutral species $Rh_2(O_2CCH_3)_2(pynp)_2$ begins to decompose upon occupation of the antibonding LUMO orbital.

Conclusions

Extensive research over the past 40 years has been carried out on the tetracarboxylate family of compounds of general formula $M_2(O_2CCH_3)_4$ (M = Mo^{II}, Ru^{II}, Rh^{II}).[22] Although these compounds are useful starting materials for a variety of M−M bonded derivatives, their redox and electronic properties are unremarkable. In sharp contrast, the new compounds in this study with two pyridyl naphthyridine ligands in addition to two acetate ligands display very different behavior. In particular, $[Mo_2(O_2CCH_3)_2(pynp)_2][BF_4]_2\cdot 3CH_3CN$ (**1**) and $[Ru_2(O_2CCH_3)_2(pynp)_2][PF_6]_2\cdot 2CH_3OH$ (**2**) exhibit four, reversible one-electron reduction processes.[29]

Density functional theory calculations were used to identify the lowest energy transitions for the three dication species $[M_2(O_2CCH_3)_2(pynp)_2]^{2+}$; these were determined to be $\delta \rightarrow \delta^*$, M-$\pi \rightarrow$ L-π^*, and M-$\pi \rightarrow$ L-π^*, respectively. The high extinction coefficient for the $\delta \rightarrow \delta^*$ transition is attributed to an increase in the ligand character of the LUMO relative to the HOMO involved in the transition. Density functional theory single point energy calculations for pertinent reduced species were used to calculate the normalized change in orbital energies (NCOE). The NCOE values are proportional to the splitting of the two 1e$^-$ reduction potentials observed by cyclic voltammetry.

Acknowledgment. K.R.D. thanks the National Science Foundation for a PI Grant (CHE-9906583) and for the CCD X-ray equipment (CHE-9807975) and SQUID magnetometer (NSF-9974899). Support from the Welch Foundation is also gratefully acknowledged. J.R.G.-M. thanks the Ministerio de

Educación y Cultura for a postdoctoral fellowship. We would like to thank the Laboratory for Molecular Simulation at Texas A&M University for providing software and computer time for the theoretical calculations along with the Supercomputing Facility at Texas A&M University for computer time. We would also like to thank Dr. Michael B. Hall for insightful discussions on correlating the calculated orbital energies with the experimental electrochemistry and Dr. Jitendra Bera for helpful comments on the manuscript.

Supporting Information Available: Additional crystallographic information. This material is available free of charge via the Internet at http://pubs.acs.org.

IC010996U